Gating transitions in the selectivity filter region of a sodium channel are coupled to the domain IV voltage sensor

Deborah L. Capes[a,b], Manoel Arcisio-Miranda[a,c], Brian W. Jarecki[a], Robert J. French[d], and Baron Chanda[a,1]

[a]Department of Neuroscience, University of Wisconsin, Madison, WI 53706; [b]Molecular and Cellular Pharmacology Graduate Program, and [c]Department of Biophysics, Federal University of Sao Paulo, 04023-060, Sao Paulo, Brazil; and [d]Department of Physiology and Pharmacology, University of Calgary, Calgary, AB, Canada T2N 4N1

Edited by Richard W. Aldrich, University of Texas, Austin, TX, and approved January 5, 2012 (received for review September 22, 2011)

Voltage-dependent ion channels are crucial for generation and propagation of electrical activity in biological systems. The primary mechanism for voltage transduction in these proteins involves the movement of a voltage-sensing domain (D), which opens a gate located on the cytoplasmic side. A distinct conformational change in the selectivity filter near the extracellular side has been implicated in slow inactivation gating, which is important for spike frequency adaptation in neural circuits. However, it remains an open question whether gating transitions in the selectivity filter region are also actuated by voltage sensors. Here, we examine conformational coupling between each of the four voltage sensors and the outer pore of a eukaryotic voltage-dependent sodium channel. The voltage sensors of these sodium channels are not structurally symmetric and exhibit functional specialization. To track the conformational rearrangements of individual voltage-sensing domains, we recorded domain-specific gating pore currents. Our data show that, of the four voltage sensors, only the domain IV voltage sensor is coupled to the conformation of the selectivity filter region of the sodium channel. Trapping the outer pore in a particular conformation with a high-affinity toxin or disulphide crossbridge impedes the return of this voltage sensor to its resting conformation. Our findings directly establish that, in addition to the canonical electromechanical coupling between voltage sensor and inner pore gates of a sodium channel, gating transitions in the selectivity filter region are also coupled to the movement of a voltage sensor. Furthermore, our results also imply that the voltage sensor of domain IV is unique in this linkage and in the ability to initiate slow inactivation in sodium channels.

electrophysiology | Nav1.4 | outer pore conformation

Voltage-gated sodium channels, like the other constituents of the voltage-gated ion channel superfamily, undergo gating transitions that result in channel opening and inactivation. Structural studies mainly on potassium selective ion channels have established that the opening of the channel primarily involves splaying of the bundle crossing formed on the intracellular side by the S6 helices (1–3). C-type inactivation gating, which follows channel opening and is mechanistically distinct from fast N-type inactivation, involves conformational rearrangements in the selectivity filter region (4–8).

According to our current thinking, inactivation gating at the selectivity filter region arises as a result of structural changes that follow pore opening and are not due to the movement of voltage sensors (9–11). Indeed, gating currents, which are a measure of voltage-sensing charge movements, are recorded under conditions with altered C-type inactivation (12) or with blockers that interact intimately with groups at the ion binding site (13, 14). For instance, the gating currents in exemplar Shaker potassium channels are typically measured in the background of the W434F mutation which results in a permanently C-type inactivated channel (15, 16). Although it has been suggested that the slow C-type inactivation may be coupled to voltage sensor movement, the evidence to date has been indirect and somewhat confounding. Charge–voltage (Q–V) curves of Shaker potassium channel were found to undergo time and voltage-dependent shifts, which correlated with development of C-type inactivation (17). Signals from fluorescent probes attached to the S3–S4 loop of the Shaker potassium channel develop an additional component, which also correlates with C-type inactivation (18). However, this may not reflect coupling between voltage sensor and outer pore because these fluorescent probes are bulky and, in all likelihood, directly sense the conformation of the outer pore. Recent studies have suggested that the holding-potential–dependent shift in the Q–V curve is an intrinsic property of a voltage sensor and may not necessarily reflect coupling to the outer pore. Charge–voltage curves of an isolated voltage sensor lacking a pore domain (D) were found to exhibit these charge shifts ("mode shifts") upon changing the holding potential (19). Moreover, a noninactivating mutant of the human ether-a-go-go related gene (HERG) channel (20) and noninactivating hyperpolarization-activated cyclic nucleotide-gated (HCN) channels (21) both show holding-potential–dependent shifts in Q–V curves. Finally, this correlation between charge shift and C-type inactivation has been reexamined by other groups who have concluded that these two processes are not coupled in the Shaker potassium channel (22).

The goal of this study is to test whether, in a voltage-gated sodium channel, the outer pore conformation is energetically coupled to the movement of a voltage sensor. As in the tetrameric potassium channels, the voltage-gated sodium channels also have two gates that control ion flux through the central pore. Studies with accessory subunits (23, 24) and local anesthetics (25, 26) provide reassuring evidence that the primary pore gate is on the cytoplasmic side of the channel. The cytoplasmic region of the β4 subunit behaves as a classical open pore blocker (1). It blocks the conductance of the open pore in a state-dependent manner and prevents the deactivation of the sodium channel gates (23). The recently solved landmark structure of a prokaryotic sodium channel, NaVab also shows rather strikingly that the intracellular pore helices can gate the ion conducting pathway (27). Several groups have proposed that the selectivity filter region of the sodium channel is the site for a second gate, which is involved in slow and ultraslow inactivation gating (28–36). In many respects, slow inactivation gating in the sodium channels is similar to C-type inactivation (4, 5, 28, 34, 35). Although residues

Author contributions: D.L.C., M.A.-M., and B.C. designed research; D.L.C., M.A.-M., and B.W.J. performed research; R.J.F. contributed new reagents/analytic tools; D.L.C., M.A.-M., B.W.J., and B.C. analyzed data; and D.L.C. and B.C. wrote the paper.

The authors declare no conflict of interest.

This article is a PNAS Direct Submission.

[1]To whom correspondence should be addressed. E-mail: chanda@wisc.edu.

This article contains supporting information online at www.pnas.org/lookup/suppl/doi:10.1073/pnas.1115575109/-/DCSupplemental.

in the intracellular S6 segments of the sodium channels have also been implicated in slow inactivation (37, 38), recent evidence with disulphide crosslinking of paired substituted cysteines strongly suggests that the occlusion of outer pore is a critical determinant for slow inactivation (31, 32). Here, we examine the coupling between the individual voltage sensors of a sodium channel and conformational rearrangements in the selectivity filter region. Using disulphide crossbridge of pore residues and high-affinity toxins, we establish that modulation of the selectivity filter conformation specifically modifies the activation of the domain IV (DIV) voltage sensor, thus implying that these two processes are conformationally coupled.

Results and Discussion

Gating Pore Currents in Charge Neutralized Mutants. To monitor the conformation of individual voltage sensors, we generated a series of mutants in which the first two or three extracellular charges of one voltage sensor at a time were mutated to a glutamine (Fig. 1*A*). Design of these *charge neutralized* (CN) Nav1.4 mutants, e.g., domain I (DI-CN) was motivated in part by recent findings that mutation of specific charged residues in the S4 segments allows state-dependent ion flux through the voltage-sensing domains (39–42). These currents directly report the movement of voltage sensors and are referred to as gating pore currents (also omega currents) to distinguish them from the canonical ionic currents through the central pore.

Each of the CN mutants, when expressed in *Xenopus* oocytes, generate currents upon depolarization resembling the wild-type sodium currents (Fig. 1*B*) (43). Due to low expression as well as persistent outward leak, we used the DII-CN mutant in which only the first two charges are neutralized for the remainder of this study. In addition to typical sodium currents, we observe large hyperpolarization activated inward currents in all CN mutants (Fig. 2). The kinetics and voltage dependence of these currents are similar to the gating pore currents reported for domain II (41).

This approach of monitoring individual voltage sensors overcomes the limitations of using large spectroscopic probes to monitor local conformational dynamics (44, 45). The fluorescent probes attached to the voltage sensors are in close proximity to the outer pore (the top of S5 and S6 segments) and, therefore, one cannot unambiguously ascribe those signals to voltage sensor movements (18).

Effect of Pore Blocking Toxins on Gating Pore Currents. To probe the coupling between the selectivity filter and the voltage sensors, we first examined the effect of tetrodotoxin (TTX), a high-affinity sodium channel blocker, because it has been reported to inhibit sodium currents in a use-dependent manner (46, 47). In CN mutants, the currents elicited by depolarizing voltage steps were completely blocked by a saturating concentration of TTX (up to 1.1 μM) (Fig. S1). As expected, TTX does not block gating pore currents through the CN mutants (41, 42). Nonetheless, to our surprise, the gating pore currents through DIV-CN were significantly altered by TTX (Fig. 2). At −110 mV, the

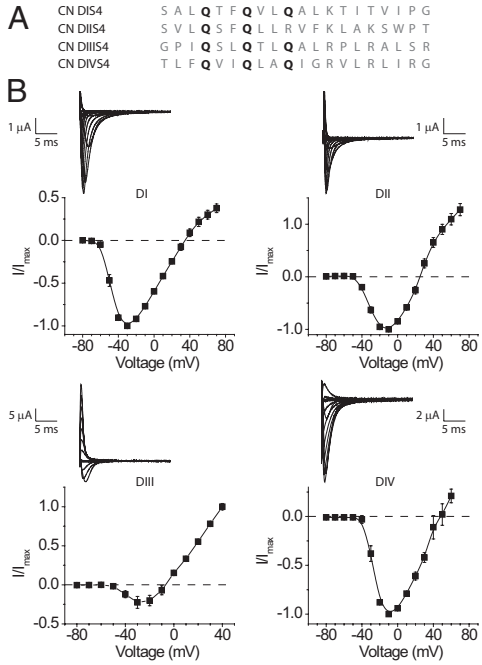

Fig. 1. Functionality of the charge-neutralized sodium channel mutants. (*A*) The sequence of the altered S4 segments of all four mutants. The sites that were mutated to glutamines are bold. (*B*) Current–voltage relationships for each of the mutants with a representative family of traces. Note that some of these current recordings were obtained in different ionic conditions (for details see *Methods*). Each graph represents the mean ± SE of at least three independent experiments. Also note that the ionic currents at more depolarized potentials are, in some cases, contaminated by gating currents.

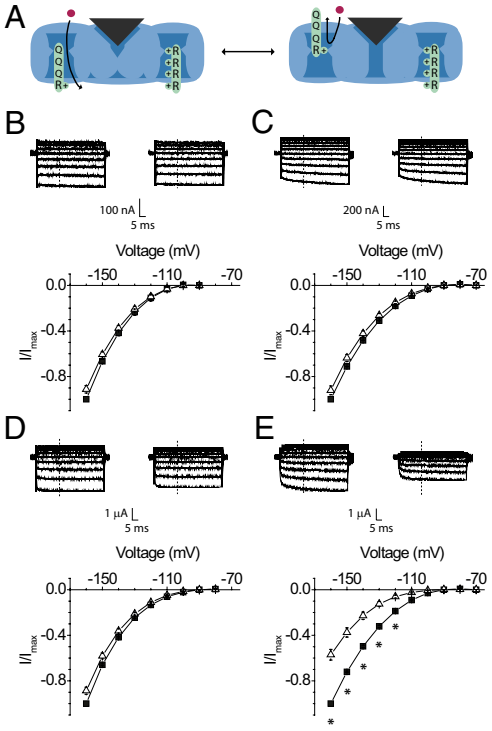

Fig. 2. Effect of TTX on gating pore currents through the individual voltage sensors. (*A*) Schematic diagram depicting the conformational processes that produce voltage-dependent gating pore currents. (*Left*) Channel where the main pore is closed and the voltage sensors are in a resting conformation. In this condition, the mutant voltage sensor is in a permissive position for gating pore currents. Currents through the central pore are blocked by a pore toxin. (*Right*) Channel with the voltage sensors in an activated conformation and the remaining charges in the mutant voltage sensor move into a position that blocks the flux of gating pore current. A family of gating pore currents before (*Left*; filled square) and after (*Right*; unfilled triangle) addition of TTX from the DI-CN (*B*), DII-CN (*C*), DIII-CN (*D*), and DIV-CN (*E*) mutants (*Upper*). Normalized current–voltage plots of the same (*Lower*). The currents at each voltage were measured at the end of 20 ms, marked as a dashed line. Each plot represents the mean ± SE of at least three independent experiments. **P* value <0.05, statistical significance.

magnitude of current was reduced by as much as 65%. Moreover, a further increase in toxin concentration (up to 10-fold) did not increase inhibition of gating pore currents, suggesting that this effect is saturated (Fig. S2). We can eliminate the possibility that the hyperpolarization activated currents through DIV-CN are due to ion flux through the central pore as opposed to being gating pore currents because the central pore currents remain completely blocked by TTX (Fig. S1). Therefore, we consider the possibility that TTX is somehow modifying the currents fluxing through gating pore within the DIV voltage sensor.

First, we examined the possibility that TTX binds directly to the voltage sensor in the DIV-CN mutant. We introduced a pore mutation at a site known to be critical for TTX binding (Y401S) in the background of the DIV-CN mutant. The Y401S mutation, located next to the selectivity determining DEKA (D400, E755, K1237, A1529) locus (48–52), yields a channel that is nearly insensitive to block by TTX (53, 54). In this background (Y401S DIV-CN), TTX had no effect on gating pore currents through the DIV voltage sensor (Fig. S3). Therefore, TTX likely influences the gating pore currents through the DIV voltage sensor by binding to the outer pore of the sodium channel.

Next, we considered the possibility that TTX interacts directly with the charged voltage sensor while being docked to its binding site in the outer pore. The highly charged pore blocking peptide, μ-conotoxin (μ-CTX), has been previously suggested to shift the voltage dependence of activation by a small degree by modifying the surface charge (55). Our prediction will be that μ-CTX, which has a nominal net charge of +6 at neutral pH, will have a much larger effect on gating pore currents if these interactions are determined solely by electrostatics (56). We observed that the saturating concentrations of μ-CTX cause a much smaller reduction (16% at most) in the DIV-CN gating pore currents (Fig. 3 and Fig. S1). These findings and others (57) support the notion that TTX perturbs the DIV voltage sensor through a mechanism that is unlikely to involve direct electrostatic interaction.

A plot of residual gating pore currents versus voltage reveals that μ-CTX inhibition of the gating pore currents is voltage independent, whereas TTX block is pronounced at depolarized potentials (Fig. S4). The voltage dependence of the block is not due to differences in voltage-dependent binding because these measurements were obtained at saturating concentrations of TTX (central pore currents remain fully blocked). Therefore, this voltage dependence reflects the effect of TTX on the gating transition of the voltage sensor and shows that TTX binding favors the activated state of the DIV voltage sensor.

TTX Modulates Off-Gating Currents. Whereas gating pore current data suggest that TTX specifically modulates the gating pore currents and by extension the voltage sensor movement, we sought to validate this observation independently. Alternate approaches to monitor conformational rearrangement of the voltage sensors involve measuring gating currents or fluorescence signals from site-specific probes. Gating currents are the most direct measure of voltage sensor movements but recording them in absence of pore blockers remains technically demanding.

To eliminate contamination due to ionic currents, we measured the off-gating currents in the wild-type channels after a depolarizing pulse sufficient to induce fast inactivation. Permeant ions in the external solution were substituted by *N*-methyl D-glucamine (NMG) to eliminate any ionic current contamination of tail currents. Robust nonlinear charge movements were recorded from the wild-type channel without pore blockers (Fig. S5) and, as expected, the charge–voltage curves obtained from these measurements were saturated at extreme potentials. A comparison of the off-gating currents before and after addition of saturating concentrations of TTX shows that the total off-gating charge is reduced by 24% (Fig. 4). Note that a substantial shift in the *Q–V* curve to a more hyperpolarized potential in the presence of TTX would result in subtraction of some of the nonlinear charge component and will be manifested as a reduced gating charge. As opposed to TTX, μ-CTX caused no reduction in the total gating charge, consistent with its effect on gating pore currents through the DIV voltage sensor (Fig. 4).

The above differences in perturbation of voltage sensor movements by the two toxins may reflect differences in their binding site or their state dependence. Remarkably, both TTX and μ-CTX can be simultaneously accommodated in the pore and, furthermore, TTX can be trapped in its binding site by μ-CTX (58, 59). The mutagenesis data also suggest that the critical residues implicated in TTX binding is in the narrow ion access pathway in the selectivity filter region (53, 54, 60). Because TTX causes a reduction in the total charge of the off-gating currents and influences the behavior of the DIV voltage sensor to a much greater extent than μ-CTX, we suggest that μ-CTX may be a more appropriate tool for collecting sodium channel gating currents. In summary, these gating current experiments establish that the TTX binding in the selectivity filter region of the sodium channel influences the movements of one or more voltage sensors of the sodium channel.

Cross-Bridging in the Selectivity Filter Affects the DIV Voltage Sensor. One possible explanation for such cross-talk is that the central pore toxins introduce a nonnative interaction that perturbs the conformation of the DIV voltage sensor. Alternatively, this long-range interaction may reflect an inherent allosteric coupling between the outer pore and this particular voltage sensor (61).

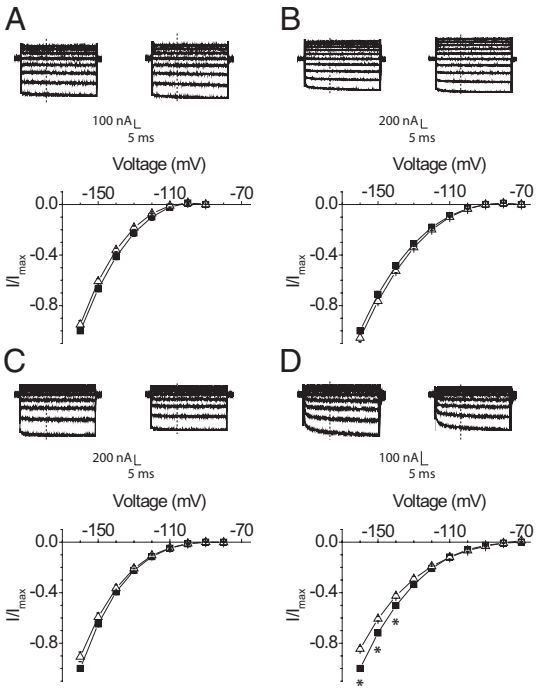

Fig. 3. Effect of μ-CTX on gating pore currents through the individual voltage sensors. A family of hyperpolarization activated currents before (*Left*; filled square) and after (*Right*; unfilled triangle) addition of μ-CTX from the DI-CN (*A*), DII-CN (*B*), DIII-CN (*C*), and DIV-CN (*D*) mutants (*Upper*). Normalized current–voltage plots of the same (*Lower*). Currents were recorded and normalized following the protocol described in *Methods*. Currents at each voltage were measured at the end of 20 ms, marked as a dashed line. Each plot represents the mean ± SE of at least three independent experiments. **P* value <0.05, statistical significance.

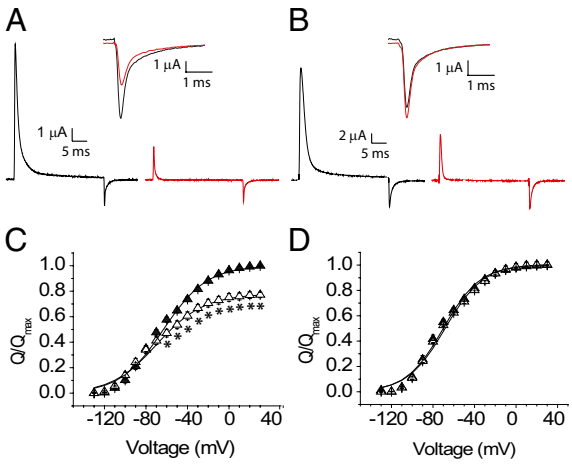

Fig. 4. Off-gating currents from the wild-type sodium channel in absence and presence of outer pore blockers. (*A*) Wild-type off-gating currents before (black trace) and after (red trace) TTX. (*Inset*) Off-gating current traces on an enlarged scale. (*B*) Wild-type off-gating currents before (black trace) and after (red trace) μ-CTX. (*Inset*) Off-gating current traces are shown enlarged. (*C*) Charge–voltage curves of the wild-type channel in the presence (filled triangle) and absence (unfilled triangle) of TTX. Each plot represents the mean ± SE of at least four independent experiments. See *Methods* for a description of the protocol. **P* < 0.01, statistical significance. (*D*) Charge–voltage curves of the wild-type channel before (filled triangle) and after (unfilled triangle) block of sodium currents by μ-CTX, shown as in *C*.

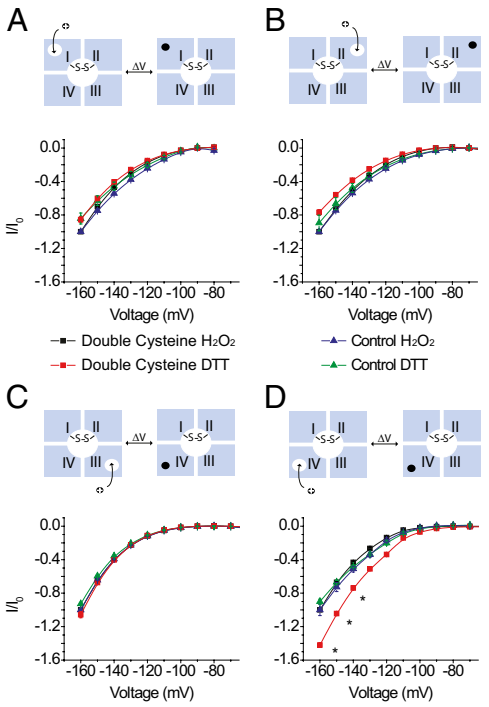

Fig. 5. Effect of disulphide cross-bridge formation in the outer pore of the sodium channel on gating pore currents through DI, DII, DIII, and DIV voltage sensors. Above each panel, a schematic diagram depicting gating pore currents through individual voltage sensors is shown. Upon depolarization, the gating pores in individual domains close, which allowed us to monitor the conformational movements of individual domains. In all cases, the pore is trapped in an inactivated conformation by disulphide cross-linking. (*A*) Normalized current–voltage plots of D400C/E755C DI-CN gating pore currents in H_2O_2 (black squares) and DTT (red squares) compared with the DI-CN control in H_2O_2 (blue triangles) and DTT (green triangles). (*B*) Normalized current–voltage plots of D400C/E755C DII-CN gating pore currents compared with those of DII-CN. Symbols are as in *A*. (*C*) Normalized current–voltage curves of D400C/E755C DIII-CN gating pore currents compared with the DIII-CN control. The symbols are the same as in *A*. (*D*) Normalized current–voltage curves of D400C/E755C DIV-CN gating pore currents compared with those of the DIV-CN control. Each plot represents the mean ± SE of at least three independent experiments. I_o refers to the H_2O_2 traces collected at −160 mV. Data were normalized to I_o for the controls and for the double cysteine mutants. **P* value <0.03, statistical significance.

To discriminate between these two possible scenarios, we used the disulphide trapping method (62). Paired cysteine substitutions in the selectivity filter region of the sodium channel form a disulphide cross-bridge and high-affinity Cd^{2+} binding sites in a state-dependent manner (30–32, 63, 64). We hypothesize that disulphide cross-linking within the pore region may prevent relative structural rearrangements and reveal intrinsic conformational coupling between the pore and the voltage sensors.

We generated a double cysteine mutant (D400C/E755C) in the background of DI, DII, DIII, and DIV-CN. These two residues constitute part of the DEKA locus in the selectivity filter region of the sodium channel and spontaneously form a disulphide cross-bridge, resulting in block of sodium currents (63). Ion conduction recovers when this cross-bridge is broken under reducing conditions. In our case, we observe small sodium currents in oocytes expressing our mutants and these currents were abolished upon addition of 4 mM H_2O_2 (Fig. S6). Under reducing conditions (1 mm dithiothreitol, DTT), we recorded robust sodium currents upon depolarization, which indicated that the cysteine cross-bridge was broken. Comparison of gating pore currents through the D400C/E755C DI, DII, and DIII mutants in reducing and oxidizing conditions showed little change (Fig. 5 *A*–*C*, respectively), whereas the gating pore currents of D400C/E755C DIV-CN increased substantially in DTT (70% at −140 mV) (Fig. 5*D*). The effects of the disulfide bridge on the gating pore currents of DIV are not due to a direct effect of H_2O_2 or DTT because the reagents have no effect on channels lacking the D400C/E755C mutations (Fig. 5).

Conformational transitions in the selectivity filter region of the sodium channel have been implicated in slow and "ultraslow" inactivation (28–34). Our experiments directly demonstrate that the domain IV voltage sensor in the skeletal muscle sodium channel is coupled to conformational transitions in the selectivity filter region of the sodium channel. Although we cannot completely rule out the possibility that the other voltage sensors are also coupled to gating transitions in the outer pore, it is remarkable that perturbation studies have previously implicated S4-DIV as being involved in slow inactivation (61). We find that prolonged depolarizations that promote slow inactivation in sodium channels inhibit gating pore currents through the domain IV voltage sensor (Fig. S7). This correlation suggests that the movement of the DIV voltage sensor may be linked to entry into the slow inactivated state. However, we should note that the reduction in the DIV gating pore currents after long depolarizations could be due to an intrinsic voltage sensor mode shift as was observed in isolated voltage sensors (19).

Mutations in domain IV also specifically affect the binding of anticonvulsants to neuronal sodium channels (65). These drugs bind to the pore in an activity-dependent manner when applied to the external side but not to the internal side (66). Moreover, TTX, which binds close to putative selectivity filter of the sodium channel, is also known to block in a use-dependent manner (67, 68). These intriguing findings are consistent with the notion established herein that the domain IV voltage sensor and outer pore of the sodium channel are conformationally coupled. The present findings are in contrast to the prevalent view that movement of the voltage sensors is exclusively coupled to opening of cytoplasmic pore gates. Furthermore, our results provide an example in which this anomalous electromechanical coupling exists

concurrently with canonical voltage sensor pore coupling. These mechanistic differences in coupling may underpin functional specialization of sodium channel domains (43, 69–72) and may be a universal feature of other nonsymmetric voltage-dependent ion channels.

Methods

Molecular Biology and Expression. Mutations were made using the QuikChange mutagenesis kit (Stratagene). cRNA was made using the mMessage mMachine T7 kit (Ambion) after digesting the plasmids containing the sodium channel gene with NotI enzyme. For heterologous expression, 50 nL of cRNA containing a mixture of α- and β1-subunit in 1:1 stoichiometry was injected into stage IV or V *Xenopus laevis* oocytes. After injection, the oocytes were kept at 18 °C in 1 × standard oocyte solution with Ca^{2+} and gentamicin for 2–5 d before recording.

Electrophysiology. Recordings were made using the cut-open oocyte voltage clamp configuration with CA-1B amplifier (Dagan) as described previously (73). Gating and ionic currents were sampled at 250 kHz with a Digidata 1400 interface (MDS Analytical Technologies) and low-pass filtered at 20 kHz. The oocytes were clamped at a holding potential of −80 mV for at least 5 min before recording. Current–voltage curves for DI, DIV-CN, and DIV-CN Y401S were obtained in 105 mM Na^+-Mes (methanesulfonic acid) external solution, whereas those for DII-CN and DIII-CN mutants were obtained in an external solution containing either 52.5 mM Na^+-Mes or 105 mM K^+-Mes, respectively. Following a 50-ms prepulse to −120 mV, the currents were elicited by test pulses ranging from −80 to +70 mV for a duration of 60 ms. Gating pore currents were recorded in 105 mM Na^+-Mes for both DI and DIV-CN, whereas the gating pore currents for DII-CN and DIII-CN were recorded in 105 mM K^+-Mes external solution with 10 mM Hepes and 2 mM $Ca(OH)_2$ at pH 7.4. Unless stated otherwise, these recordings used NMG-Mes internal solution with 105 mM NMG, 10 mM Hepes, and 2 mM EGTA at pH 7.4. Gating pore currents were elicited by test pulses from −160 to −70 mV for 60 ms following a 50-ms prepulse to −120 mV. The currents were normalized with respect to the maximum current measured before toxin, typically at −160 mV. Channels were blocked using 0.6–1.1 μM of TTX or 6–25.7 μM of μ-CTX in the external solutions. Gating pore currents were recorded without a P/4 subtraction protocol, which means that the activation kinetics were likely to be contaminated by capacity transients. Offline leak subtraction was used to eliminate the linear leak component in experiments where it was significant (74).

To record the off-gating currents, we applied a prepulse to +50 mV for 30 ms to inactivate the channels. This was followed by a test pulse to potentials ranging from −130 mV to +50 mV for 20-ms durations. These experiments were performed in NMG-Mes internal and external (105 mM NMG-Mes with 10 mM Hepes, and 2 mM $Ca(OH)_2$) solutions. To obtain gating currents in presence of toxin, 0.6–1.1 μM TTX or 6–25.7 μM μ-CTX was added to the external solution. At these concentrations, ionic currents were fully blocked. The charge–voltage curves for the off-gating currents were fit to a single Boltzmann equation: $Q/Q_{max}(V) = 1/(1 + \exp(-ze(V - V_{1/2})/KT))$ to estimate the $V_{1/2}$ (voltage for half-maximal activation) and z (valence) values. Linear capacity transients were eliminated by P/−4 subtraction at a holding potential of −130 mV.

For cross-linking experiments, the oocytes expressing mutants were treated with 2 mM H_2O_2 to maximize the disulfide formation. To measure currents under reducing conditions, 1 mM of freshly made DTT was added to the external solution containing 105 mM Na^+-Mes.

ACKNOWLEDGMENTS. We thank K. M. Schuldt for technical assistance with Na_V channel mutants and the members of the B.C. laboratory, Meyer Jackson, and Francisco Bezanilla for their valuable comments. This work was supported by National Institutes of Health training grants (to D.L.C. and B.W.J.), Grant R01-GM084140 (to B.C.), and the Shaw Scientist Award (to B.C.).

1. Armstrong CM (1966) Time course of TEA(+)-induced anomalous rectification in squid giant axons. *J Gen Physiol* 50:491–503.
2. Liu Y, Holmgren M, Jurman ME, Yellen G (1997) Gated access to the pore of a voltage-dependent K+ channel. *Neuron* 19:175–184.
3. Jiang Y, et al. (2002) The open pore conformation of potassium channels. *Nature* 417: 523–526.
4. Liu Y, Jurman ME, Yellen G (1996) Dynamic rearrangement of the outer mouth of a K+ channel during gating. *Neuron* 16:859–867.
5. López-Barneo J, Hoshi T, Heinemann SH, Aldrich RW (1993) Effects of external cations and mutations in the pore region on C-type inactivation of Shaker potassium channels. *Receptors Channels* 1:61–71.
6. Cordero-Morales JF, et al. (2006) Molecular determinants of gating at the potassium-channel selectivity filter. *Nat Struct Mol Biol* 13:311–318.
7. Cordero-Morales JF, Cuello LG, Perozo E (2006) Voltage-dependent gating at the KcsA selectivity filter. *Nat Struct Mol Biol* 13:319–322.
8. Cuello LG, Jogini V, Cortes DM, Perozo E (2010) Structural mechanism of C-type inactivation in K(+) channels. *Nature* 466:203–208.
9. Panyi G, Deutsch C (2006) Cross talk between activation and slow inactivation gates of Shaker potassium channels. *J Gen Physiol* 128:547–559.
10. Panyi G, Deutsch C (2007) Probing the cavity of the slow inactivated conformation of shaker potassium channels. *J Gen Physiol* 129:403–418.
11. Cuello LG, et al. (2010) Structural basis for the coupling between activation and inactivation gates in K(+) channels. *Nature* 466:272–275.
12. Perozo EMR, MacKinnon R, Bezanilla F, Stefani E (1993) Gating currents from a nonconducting mutant reveal open-closed conformations in Shaker K+ channels. *Neuron* 11:353–358.
13. Armstrong CM, Bezanilla F (1974) Charge movement associated with the opening and closing of the activation gates of the Na channels. *J Gen Physiol* 63:533–552.
14. Heginbotham L, MacKinnon R (1992) The aromatic binding site for tetraethylammonium ion on potassium channels. *Neuron* 8:483–491.
15. Yang Y, Yan Y, Sigworth FJ (1997) How does the W434F mutation block current in Shaker potassium channels? *J Gen Physiol* 109:779–789.
16. Starkus JG, Kuschel L, Rayner MD, Heinemann SH (1998) Macroscopic Na+ currents in the "Nonconducting" Shaker potassium channel mutant W434F. *J Gen Physiol* 112: 85–93.
17. Olcese R, Latorre R, Toro L, Bezanilla F, Stefani E (1997) Correlation between charge movement and ionic current during slow inactivation in Shaker K+ channels. *J Gen Physiol* 110:579–589.
18. Loots E, Isacoff EY (1998) Protein rearrangements underlying slow inactivation of the Shaker K+ channel. *J Gen Physiol* 112:377–389.
19. Villalba-Galea CA, Sandtner W, Starace DM, Bezanilla F (2008) S4-based voltage sensors have three major conformations. *Proc Natl Acad Sci USA* 105:17600–17607.
20. Piper DR, Varghese A, Sanguinetti MC, Tristani-Firouzi M (2003) Gating currents associated with intramembrane charge displacement in HERG potassium channels. *Proc Natl Acad Sci USA* 100:10534–10539.
21. Männikkö R, Pandey S, Larsson HP, Elinder F (2005) Hysteresis in the voltage dependence of HCN channels: Conversion between two modes affects pacemaker properties. *J Gen Physiol* 125:305–326.
22. Haddad GA, Blunck R (2011) Mode shift of the voltage sensors in Shaker K+ channels is caused by energetic coupling to the pore domain. *J Gen Physiol* 137:455–472.
23. Raman IM, Bean BP (2001) Inactivation and recovery of sodium currents in cerebellar Purkinje neurons: Evidence for two mechanisms. *Biophys J* 80:729–737.
24. Grieco TM, Malhotra JD, Chen C, Isom LL, Raman IM (2005) Open-channel block by the cytoplasmic tail of sodium channel beta4 as a mechanism for resurgent sodium current. *Neuron* 45:233–244.
25. Hille B (1977) Local anesthetics: Hydrophilic and hydrophobic pathways for the drug-receptor reaction. *J Gen Physiol* 69:497–515.
26. Wang SY, Mitchell J, Moczydlowski E, Wang GK (2004) Block of inactivation-deficient Na+ channels by local anesthetics in stably transfected mammalian cells: Evidence for drug binding along the activation pathway. *J Gen Physiol* 124:691–701.
27. Payandeh J, Scheuer T, Zheng N, Catterall WA (2011) The crystal structure of a voltage-gated sodium channel. *Nature* 475:353–358.
28. Balser JR, et al. (1996) External pore residue mediates slow inactivation in mu 1 rat skeletal muscle sodium channels. *J Physiol* 494:431–442.
29. Bénitah JP, Chen Z, Balser JR, Tomaselli GF, Marbán E (1999) Molecular dynamics of the sodium channel pore vary with gating: Interactions between P-segment motions and inactivation. *J Neurosci* 19:1577–1585.
30. Ong BH, Tomaselli GF, Balser JR (2000) A structural rearrangement in the sodium channel pore linked to slow inactivation and use dependence. *J Gen Physiol* 116: 653–662.
31. Xiong W, et al. (2006) A conserved ring of charge in mammalian Na+ channels: A molecular regulator of the outer pore conformation during slow inactivation. *J Physiol* 576:739–754.
32. Xiong W, Li RA, Tian Y, Tomaselli GF (2003) Molecular motions of the outer ring of charge of the sodium channel: Do they couple to slow inactivation? *J Gen Physiol* 122: 323–332.
33. Todt H, Dudley SC, Jr., Kyle JW, French RJ, Fozzard HA (1999) Ultra-slow inactivation in mu1 Na+ channels is produced by a structural rearrangement of the outer vestibule. *Biophys J* 76:1335–1345.
34. Townsend C, Horn R (1997) Effect of alkali metal cations on slow inactivation of cardiac Na+ channels. *J Gen Physiol* 110:23–33.
35. Vilin YY, Fujimoto E, Ruben PC (2001) A single residue differentiates between human cardiac and skeletal muscle Na+ channel slow inactivation. *Biophys J* 80:2221–2230.
36. Hilber K, et al. (2001) The selectivity filter of the voltage-gated sodium channel is involved in channel activation. *J Biol Chem* 276:27831–27839.
37. Vedantham V, Cannon SC (2000) Rapid and slow voltage-dependent conformational changes in segment IVS6 of voltage-gated Na(+) channels. *Biophys J* 78:2943–2958.
38. Struyk AF, Cannon SC (2002) Slow inactivation does not block the aqueous accessibility to the outer pore of voltage-gated Na channels. *J Gen Physiol* 120:509–516.
39. Starace DM, Bezanilla F (2004) A proton pore in a potassium channel voltage sensor reveals a focused electric field. *Nature* 427:548–553.

40. Tombola F, Pathak MM, Isacoff EY (2005) Voltage-sensing arginines in a potassium channel permeate and occlude cation-selective pores. *Neuron* 45:379–388.
41. Sokolov S, Scheuer T, Catterall WA (2005) Ion permeation through a voltage-sensitive gating pore in brain sodium channels having voltage sensor mutations. *Neuron* 47: 183–189.
42. Struyk AF, Cannon SC (2007) A Na+ channel mutation linked to hypokalemic periodic paralysis exposes a proton-selective gating pore. *J Gen Physiol* 130:11–20.
43. Chanda B, Bezanilla F (2002) Tracking voltage-dependent conformational changes in skeletal muscle sodium channel during activation. *J Gen Physiol* 120:629–645.
44. Horn R (2000) A new twist in the saga of charge movement in voltage-dependent ion channels. *Neuron* 25:511–514.
45. Cha A, Bezanilla F (1998) Structural implications of fluorescence quenching in the Shaker K+ channel. *J Gen Physiol* 112:391–408.
46. Patton DE, Goldin AL (1991) A voltage-dependent gating transition induces use-dependent block by tetrodotoxin of rat IIA sodium channels expressed in Xenopus oocytes. *Neuron* 7:637–647.
47. Heggeness ST, Starkus JG (1986) Saxitoxin and tetrodotoxin. Electrostatic effects on sodium channel gating current in crayfish axons. *Biophys J* 49:629–643.
48. Heinemann SH, Terlau H, Stühmer W, Imoto K, Numa S (1992) Calcium channel characteristics conferred on the sodium channel by single mutations. *Nature* 356: 441–443.
49. Favre I, Moczydlowski E, Schild L (1996) On the structural basis for ionic selectivity among Na+, K+, and Ca2+ in the voltage-gated sodium channel. *Biophys J* 71: 3110–3125.
50. Chiamvimonvat N, Pérez-García MT, Ranjan R, Marban E, Tomaselli GF (1996) Depth asymmetries of the pore-lining segments of the Na+ channel revealed by cysteine mutagenesis. *Neuron* 16:1037–1047.
51. Pérez-García MT, et al. (1997) Mechanisms of sodium/calcium selectivity in sodium channels probed by cysteine mutagenesis and sulfhydryl modification. *Biophys J* 72: 989–996.
52. Huang CJ, Favre I, Moczydlowski E (2000) Permeation of large tetra-alkylammonium cations through mutant and wild-type voltage-gated sodium channels as revealed by relief of block at high voltage. *J Gen Physiol* 115:435–454.
53. Backx PH, Yue DT, Lawrence JH, Marban E, Tomaselli GF (1992) Molecular localization of an ion-binding site within the pore of mammalian sodium channels. *Science* 257: 248–251.
54. Satin J, et al. (1992) A mutant of TTX-resistant cardiac sodium channels with TTX-sensitive properties. *Science* 256:1202–1205.
55. French RJ, et al. (1996) Interactions between a pore-blocking peptide and the voltage sensor of the sodium channel: An electrostatic approach to channel geometry. *Neuron* 16:407–413.
56. Moczydlowski E, Olivera BM, Gray WR, Strichartz GR (1986) Discrimination of muscle and neuronal Na-channel subtypes by binding competition between [3H]saxitoxin and mu-conotoxins. *Proc Natl Acad Sci USA* 83:5321–5325.
57. Moczydlowski E, Garber SS, Miller C (1984) Batrachotoxin-activated Na+ channels in planar lipid bilayers. Competition of tetrodotoxin block by Na+. *J Gen Physiol* 84: 665–686.
58. Zhang MM, et al. (2009) Synergistic and antagonistic interactions between tetrodotoxin and mu-conotoxin in blocking voltage-gated sodium channels. *Channels (Austin)* 3:32–38.
59. Zhang MM, et al. (2010) Cooccupancy of the outer vestibule of voltage-gated sodium channels by micro-conotoxin KIIIA and saxitoxin or tetrodotoxin. *J Neurophysiol* 104: 88–97.
60. Leffler A, Herzog RI, Dib-Hajj SD, Waxman SG, Cummins TR (2005) Pharmacological properties of neuronal TTX-resistant sodium channels and the role of a critical serine pore residue. *Pflugers Arch* 451:454–463.
61. Mitrovic N, George AL, Jr., Horn R (2000) Role of domain 4 in sodium channel slow inactivation. *J Gen Physiol* 115:707–718.
62. Falke JJ, Koshland DE, Jr. (1987) Global flexibility in a sensory receptor: A site-directed cross-linking approach. *Science* 237:1596–1600.
63. Bénitah JP, et al. (1997) Molecular motions within the pore of voltage-dependent sodium channels. *Biophys J* 73:603–613.
64. Tsushima RG, Li RA, Backx PH (1997) P-loop flexibility in Na+ channel pores revealed by single- and double-cysteine replacements. *J Gen Physiol* 110:59–72.
65. Yang YC, Hsieh JY, Kuo CC (2009) The external pore loop interacts with S6 and S3-S4 linker in domain 4 to assume an essential role in gating control and anticonvulsant action in the Na(+) channel. *J Gen Physiol* 134:95–113.
66. Kuo CC (1998) A common anticonvulsant binding site for phenytoin, carbamazepine, and lamotrigine in neuronal Na+ channels. *Mol Pharmacol* 54:712–721.
67. Cohen CJ, Bean BP, Colatsky TJ, Tsien RW (1981) Tetrodotoxin block of sodium channels in rabbit Purkinje fibers. Interactions between toxin binding and channel gating. *J Gen Physiol* 78:383–411.
68. Gonoi T, Sherman SJ, Catterall WA (1985) Voltage clamp analysis of tetrodotoxin-sensitive and -insensitive sodium channels in rat muscle cells developing in vitro. *J Neurosci* 5:2559–2564.
69. Bosmans F, Martin-Eauclaire MF, Swartz KJ (2008) Deconstructing voltage sensor function and pharmacology in sodium channels. *Nature* 456:202–208.
70. Horn R, Ding S, Gruber HJ (2000) Immobilizing the moving parts of voltage-gated ion channels. *J Gen Physiol* 116:461–476.
71. Sheets MF, Kyle JW, Kallen RG, Hanck DA (1999) The Na channel voltage sensor associated with inactivation is localized to the external charged residues of domain IV, S4. *Biophys J* 77:747–757.
72. Yang N, Horn R (1995) Evidence for voltage-dependent S4 movement in sodium channels. *Neuron* 15:213–218.
73. Taglialatela M, Toro L, Stefani E (1992) Novel voltage clamp to record small, fast currents from ion channels expressed in Xenopus oocytes. *Biophys J* 61:78–82.
74. Sokolov S, Scheuer T, Catterall WA (2010) Ion permeation and block of the gating pore in the voltage sensor of NaV1.4 channels with hypokalemic periodic paralysis mutations. *J Gen Physiol* 136:225–236.